**Edelweiss Applied Science and Technology**
*ISSN: 2576-8484*
*Vol. 10, No. 9, 157-173*
*2026*
*Publisher: Learning Gate*
*DOI: 10.55214/2576-8484.v10i9.13563*


# Ameliorating the performance of nanosilicon-based anode materials for alkali metal (Li, Na, K) ion battery: A promising applied technique for energy storage

Fatemeh Mollaamin[1*], Majid Monajjemi[2]
[1]Department of Biomedical Engineering, Faculty of Engineering and Architecture, Kastamonu University, Kastamonu, Turkey; fmollaamin@kastamonu.edu.tr (F.M.).
[2]Department of Biology, Faculty of Science, Kastamonu University, Kastamonu, Turkey; mmonajjemi@kastamonu.edu.tr (M.M.).

**Abstract:** Silicon carbide (SiC) has been designed and characterized as an anode electrode for lithium (Li)-, sodium (Na)-, and potassium (K)-ion batteries because it forms $Li_2$(SiC), $Na_2$(SiC), and $K_2$(SiC) nanoclusters. A comprehensive study of energy storage by $Li_2$(SiC), $Na_2$(SiC), and $K_2$(SiC) complexes was conducted using computational approaches, including density-of-states analysis, charge-density differences (CDD), total density of states (TDOS), and molecular electrostatic potential (ESP) calculations for hybrid clusters of $Li_2$(SiC), $Na_2$(SiC), and $K_2$(SiC). The entry of a small portion of Li, Na, or K into the Si–C layer to replace alkali- and alkaline-earth-metal sites could improve the structural stability of the electrode material at high multiplicity, thereby improving the capacity-retention rate. A higher Si/C content can increase battery capacity through $Li_2$(SiC), $Na_2$(SiC), and $K_2$(SiC) nanoclusters during the energy-storage process and improve rate performance by enhancing electrical conductivity. Besides, SiC anode material may advance cycling consistency by preventing electrode degradation and augmenting capacity owing to higher surface-capacitive effects.

***Keywords:*** *Alkali/alkaline earth metals, Density of states, Energy-saving, Novel hybrid-ion batteries, Silicon carbide.*

## 1. Introduction

Large-volume variation during the charge/discharge of silicon nanostructures applied as anode electrodes for high-energy lithium-ion batteries (LIBs) has been considered the most critical problem, inhibiting their commercial applications. Searching for alternative high-performance anodes for LIBs has been emphasized. Silicon carbide (SiC) nanomaterials, wide-bandgap semiconductors with excellent mechanical properties, have been investigated as anode electrode materials, either as active materials, protective layers, or inactive buffer material [1].

It is relevant to remark that Si-based inorganic compounds have been extensively examined for lithium-ion batteries (LIBs) [2]. Similarly, although Si-based polymer-derived ceramics (PDCs) have already been investigated as electrodes in rechargeable LIBs, Wen et al. [3] found no results regarding their potential for magnesium-ion batteries (MIBs). One promising anode material for LIBs is silicon (Si), with a theoretical capacity nearly ten times that of graphite [4]. However, the use of Si anodes remains limited because of significant volume expansion and pulverization during battery cycling, causing structural deterioration and poor performance stability [2]. The polymers derived from ceramics, especially those with a silicon backbone, might be a suitable candidate to address the mentioned concerns [3]. Therefore, SiOC, with Si tetrahedrally coordinated to O and C, has already been studied as an electrode in rechargeable lithium-ion batteries [5-8].

Together with the low diffusion barrier, moderate open-circuit voltage, and excellent electronic conductivity during sodiation, the researchers proposed that graphitic SiC is a potential material for Na-


**History:** Received: 11 June 2026; Revised: 17 August 2026; Accepted: 21 August 2026; Published: 7 September 2026
* Correspondence: fmollaamin@kastamonu.edu.tr

ion battery anodes. More importantly, they found that the intercalation strength of Na ions into C-based multilayer materials could be enhanced by increasing the amount of covalent components in Na–C bonds, which could be realized via doping with atoms (like Li, Be, B, Al, Si, or P) with lower electronegativity than that of C atoms [9].

The novel structure of a SiC monolayer was investigated for sodium and potassium storage using the DFT method. It was revealed that SiC exhibits negative adsorption energies for K/Na adsorption on its surface. Furthermore, the SiC monolayer can efficiently achieve a high content of Na/K loading on both sides of its surface. Additionally, it was demonstrated that the semiconducting SiC monolayer transforms into a metallic state with excellent conductivity upon Na/K adsorption. These findings underscore the potential of the SiC monolayer as a promising candidate for sodium-ion and potassium-ion batteries [10].

Anode materials based on silicon carbide and III-nitride nanosheets are investigated for magnesium-ion batteries (MIBs) as possible alternatives to lithium- and sodium-ion batteries. The calculated density functional theory results reveal higher internal energy changes and cell voltages for MIBs with silicon carbide, boron nitride, aluminum nitride, and gallium nitride anode materials than those previously reported for carbon nanomaterials [11].

Whereas the polarizability of Si is greater than that of the C atom, it is assumed that Si–C/Si nanosurfaces may contribute more intensely to hybrid compositions than to pure C nanostructures [12-14]. Previous investigations of energy-saving devices through H adsorption have been conducted using DFT calculations on semiconductor-group Si/Ge/Sn/Pb nanocarbides [15], Mg-Al nanoalloys [16], and Al/C/Si-doped BN nanocomposites [17]. Nanomaterials with notable structures address emerging demands in electrocatalysis, fuel cells, and energy-saving applications [18].

This investigation aims to explore the feasibility of $Li_2$(SiC), $Na_2$(SiC), and $K_2$(SiC) nanoclusters for energy storage. Therefore, the physicochemical properties of the aforementioned $Li_2$(SiC), $Na_2$(SiC), and $K_2$(SiC) heteroclusters were analyzed. In this context, [SiC] nanoclusters modeled with the hybrid alkali metals Li, Na, and K were considered as cathode materials for comparison. Following in-depth characterization, the samples were evaluated for their performance in relation to variations in chemical composition to assess their potential for the first time in Li-, Na-, or K-batteries.

## 2. Theory, Materials and Computation

Figures 1 a,b,c show alkali-metal-based nanoclusters, $Li_2$(SiC), $Na_2$(SiC), and $K_2$(SiC), which can enhance energy storage in battery cells, transistors, or other semiconducting devices. In this investigation, computations were conducted using the Coulomb-attenuating method (Becke, 3-parameter, Lee-Yang-Parr) [CAM–B3LYP–D3] level of theory.

*Edelweiss Applied Science and Technology*
*ISSN: 2576-8484*
*Vol. 10, No. 9: 157-173, 2026*
*DOI: 10.55214/2576-8484.v10i9.13563*

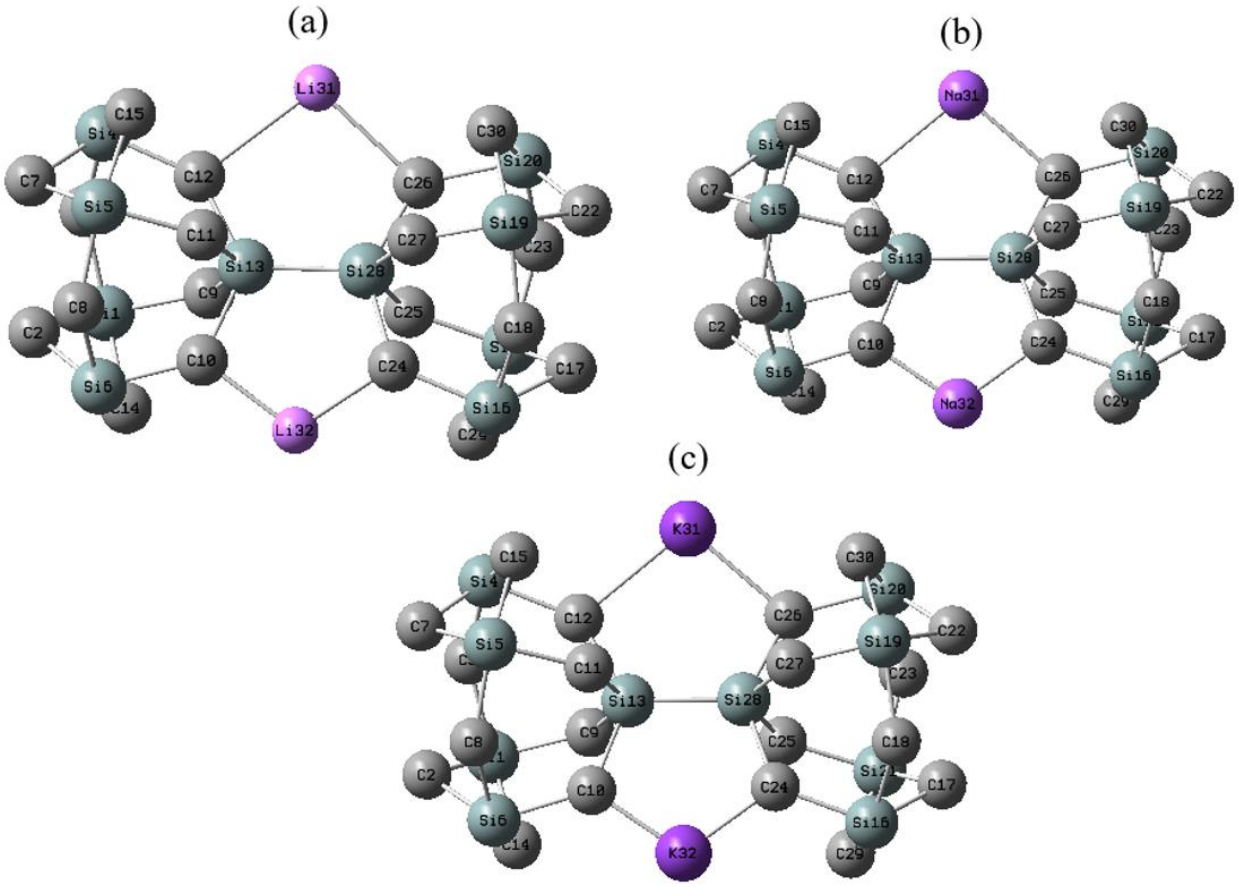


**Figure 1.**
Adding Li, Na, K to SiC nanocluster and formation of (a) $Li_2(SiC)$, (b) $Na_2(SiC)$, and (c) $K_2(SiC)$ complexes towards energy storage in novel batteries.

The analysis of the Bader charge parameter [19] has been performed for energy storage in hybrid clusters of $Li_2(SiC)$, $Na_2(SiC)$, and $K_2(SiC)$ complexes (Figure 1a,b,c) using Gaussian 16 revision C.01 computational software [20] and the GaussView 6.1 graphical program [21]. The applied basis sets for theoretical calculations of energy storage by $Li_2(SiC)$, $Na_2(SiC)$, and $K_2(SiC)$ complexes were supported by LANL2DZ and 6–311+G (d,p).

One of the most significant advantages of applying SiC nanoclusters as anodes in Li-, Na-, or K-ion batteries is that they provide several potential Li/Na/K-ion storage pathways in a stable SiC anode material, increased electrical conductivity from Si/C, and increased surface area from the nanocluster morphology. In this investigation, homogeneously distributed silicon or carbon elements can be immobilized in the SiC matrix, which prevents their tendency to form agglomerates during battery cycling. Li/Na/K insertion might also result in the cleavage of some C–Li, C–Na, or C–K bonds in the SiC anode material and its expansion, providing favorable sites for subsequent ion insertion into the network (Figure 1a,b,c). At the same time, Li, Na, or K atoms could react rapidly with silicon or carbide in SiC nanoclusters to form $Li_2(SiC)$ (Figure 1a), $Na_2(SiC)$ (Figure 1b), and $K_2(SiC)$ (Figure 1c) heteroclusters.

*Edelweiss Applied Science and Technology*
*ISSN: 2576-8484*
*Vol. 10, No. 9: 157-173, 2026*
*DOI: 10.55214/2576-8484.v10i9.13563*

## 3. Results and Discussion

*3.1. Charge Density Differences Analysis*

In Figure 2(a,b,c), charge density differences (CDD) [22] have been shown for $Li_2(SiC)$, $Na_2(SiC)$, and $K_2(SiC)$ nanoclusters, with vibrations in the region from −12 to +9 Bohr resulting from co-interactions between the alkali metals Li31–Li32, Na31–Na32, and K31–K32. Moreover, the elements C2, C3, C7–C12, C14, C15, C17, C18, C22–C27, C29, and C30 in the $Li_2(SiC)$, $Na_2(SiC)$, and $K_2(SiC)$ nanoclusters have exhibited vibrations from −12 to +9 Bohr (Figure 2a,b,c).

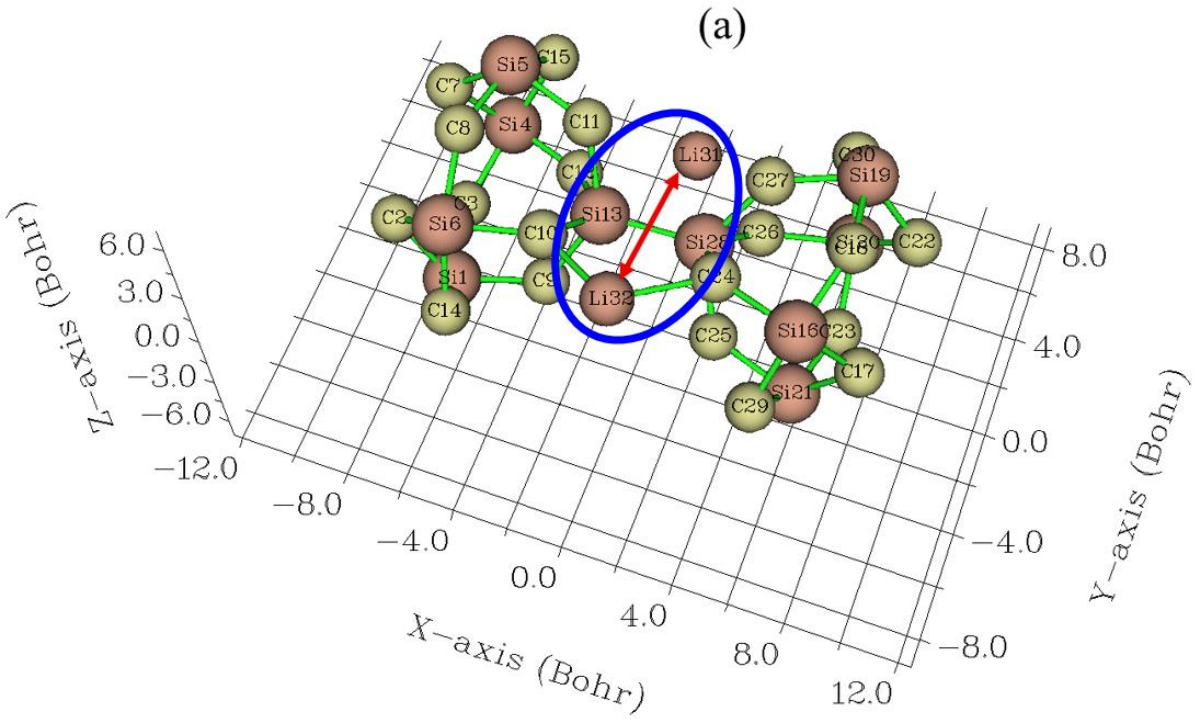


*Edelweiss Applied Science and Technology*
*ISSN: 2576-8484*
*Vol. 10, No. 9: 157-173, 2026*
*DOI: 10.55214/2576-8484.v10i9.13563*

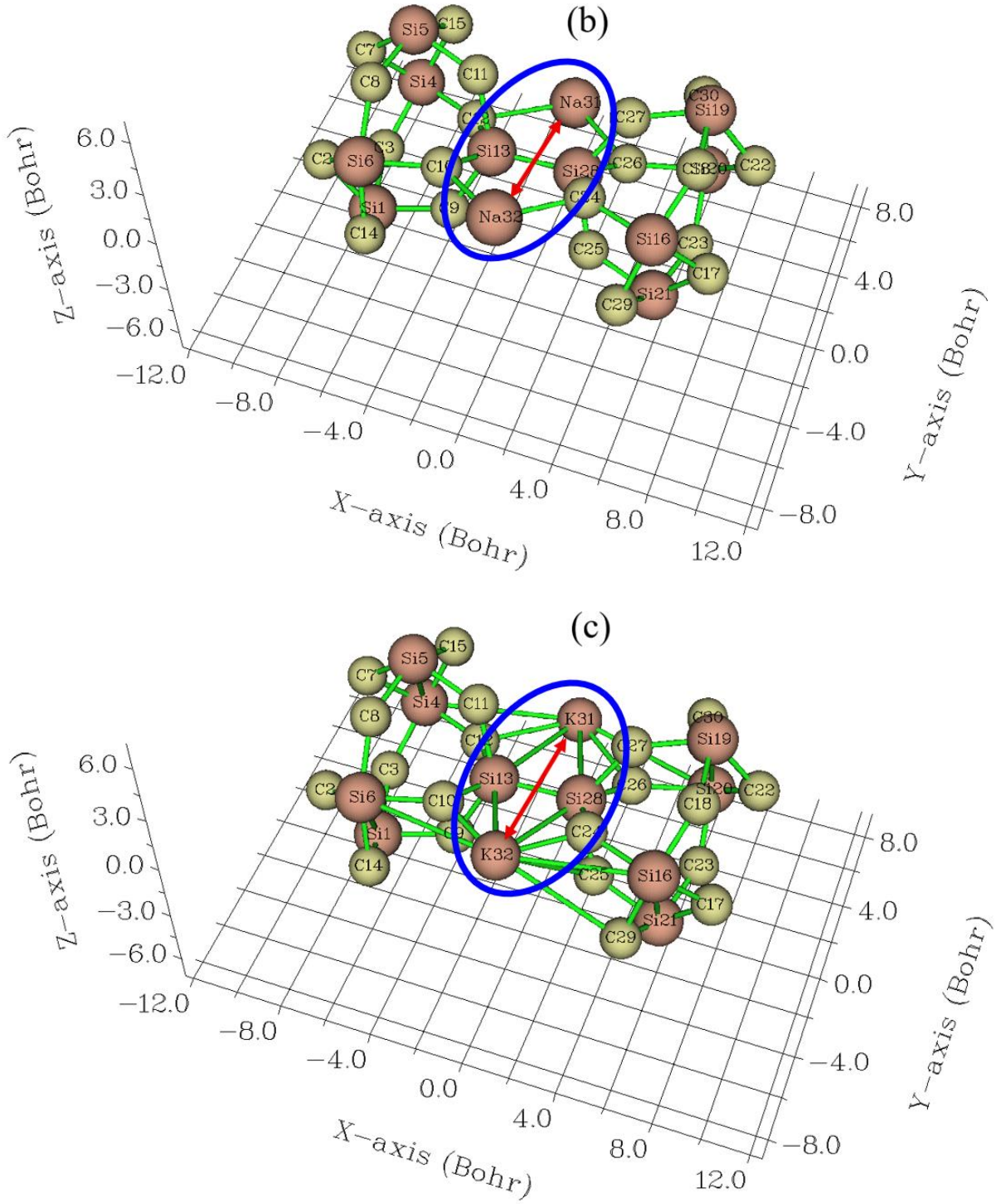


**Figure 2.**
CDD graphs for (a) $Li_2(SiC)$, (b) $Na_2(SiC)$, and (c) $K_2(SiC)$ nanoclusters.

The charge distribution of the alkali metals captured by the SiC nanostructure during the formation of $Li_2(SiC)$, $Na_2(SiC)$, and $K_2(SiC)$ nanoclusters, respectively, is illustrated in Table 1.

*Edelweiss Applied Science and Technology*
*ISSN: 2576-8484*
*Vol. 10, No. 9: 157-173, 2026*
*DOI: 10.55214/2576-8484.v10i9.13563*

**Table 1.**
The atomic charge (Q/coulomb) for $Li_2(SiC)$, $Na_2(SiC)$ and $K_2(SiC)$ nanoclusters.

| $Li_2(SiC)$ | | $Na_2(SiC)$ | | $K_2(SiC)$ | |
|---|---|---|---|---|---|
| **Atom** | **Q** | **Atom** | **Q** | **Atom** | **Q** |
| Si1 | 0.7594 | Si1 | 0.7475 | Si1 | 0.7546 |
| C2 | −0.4224 | C2 | −0.4274 | C2 | −0.4353 |
| C3 | −0.3467 | C3 | −0.3679 | C3 | −0.3436 |
| Si4 | 0.7354 | Si4 | 0.7366 | Si4 | 0.7280 |
| Si5 | 0.7337 | Si5 | 0.7460 | Si5 | 0.7494 |
| Si6 | 0.7959 | Si6 | 0.8510 | Si6 | 0.8303 |
| C7 | −0.3817 | C7 | −0.4035 | C7 | −0.3960 |
| C8 | −0.3592 | C8 | −0.3769 | C8 | −0.3680 |
| C9 | −0.3811 | C9 | −0.3700 | C9 | −0.3719 |
| C10 | −0.8081 | C10 | −0.7046 | C10 | −1.0149 |
| C11 | −0.3684 | C11 | −0.3536 | C11 | −0.3251 |
| C12 | −0.9272 | C12 | −0.8236 | C12 | −0.9041 |
| Si13 | 1.1158 | Si13 | 0.9622 | Si13 | 0.9949 |
| C14 | −0.3680 | C14 | −0.3679 | C14 | −0.3640 |
| C15 | −0.3823 | C15 | −0.3858 | C15 | −0.4090 |
| Si16 | 0.8138 | Si16 | 0.8591 | Si16 | 0.8606 |
| C17 | −0.4172 | C17 | −0.4239 | C17 | −0.4355 |
| C18 | −0.3541 | C18 | −0.3704 | C18 | −0.3799 |
| Si19 | 0.7121 | Si19 | 0.7087 | Si19 | 0.7040 |
| Si20 | 0.7500 | Si20 | 0.7765 | Si20 | 0.7468 |
| Si21 | 0.7663 | Si21 | 0.7543 | Si21 | 0.7536 |
| C22 | −0.3827 | C22 | −0.4001 | C22 | −0.4006 |
| C23 | −0.3470 | C23 | −0.3835 | C23 | −0.3643 |
| C24 | −0.7862 | C24 | −0.6938 | C24 | −0.9674 |
| C25 | −0.3396 | C25 | −0.3439 | C25 | −0.3215 |
| C26 | −0.8547 | C26 | −0.7516 | C26 | −0.9120 |
| C27 | −0.5091 | C27 | −0.4721 | C27 | −0.4640 |
| Si28 | 1.0727 | Si28 | 1.0081 | Si28 | 1.0416 |
| C29 | −0.3982 | C29 | −0.3959 | C29 | −0.4276 |
| C30 | −0.3747 | C30 | −0.3908 | C30 | −0.3754 |
| Li31 | 0.7519 | Na31 | 0.6846 | K31 | 0.9090 |
| Li32 | 0.5019 | Na32 | 0.3727 | K32 | 0.9075 |

Functionalization with Li, Na, and K atoms can increase the negative atomic charges of C2, C3, C7–C12, C14, C15, C17, C18, C22–C27, C29, and C30, enabling them to act as electron acceptors in $Li_2(SiC)$, $Na_2(SiC)$, and $K_2(SiC)$ nanoclusters (Figure 3a,b,c).

*Edelweiss Applied Science and Technology*
*ISSN: 2576-8484*
*Vol. 10, No. 9: 157-173, 2026*
*DOI: 10.55214/2576-8484.v10i9.13563*

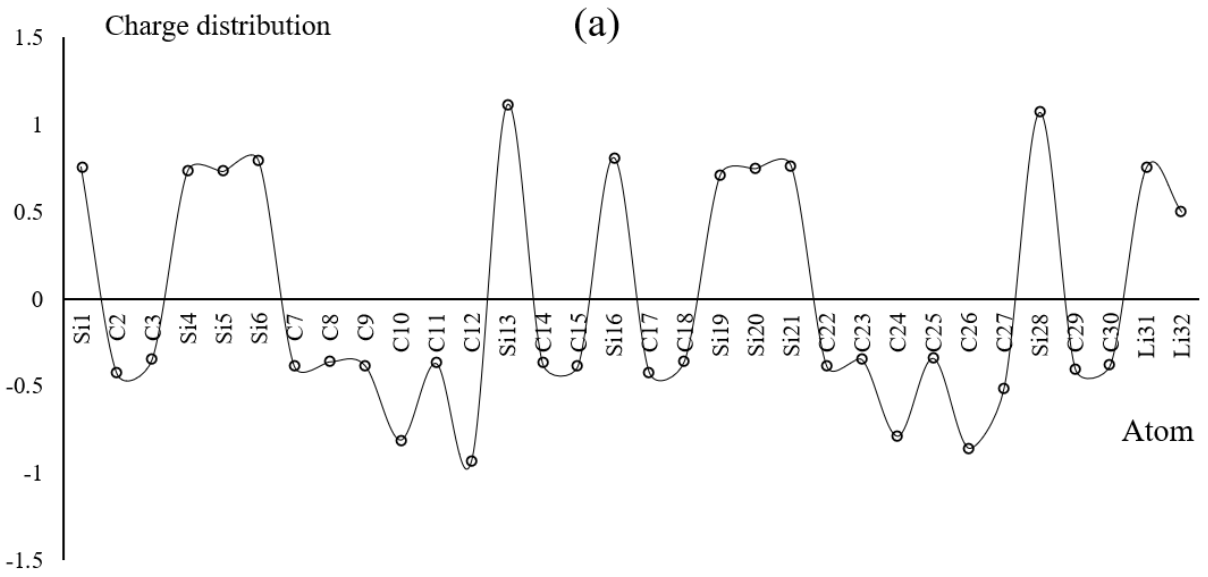


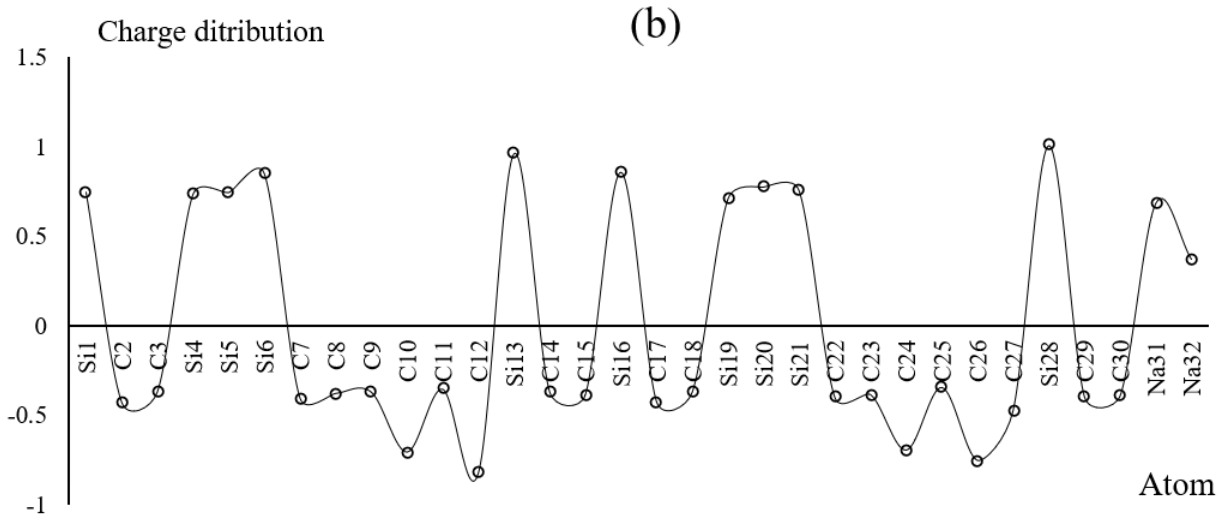


*Edelweiss Applied Science and Technology*
*ISSN: 2576-8484*
*Vol. 10, No. 9: 157-173, 2026*
*DOI: 10.55214/2576-8484.v10i9.13563*

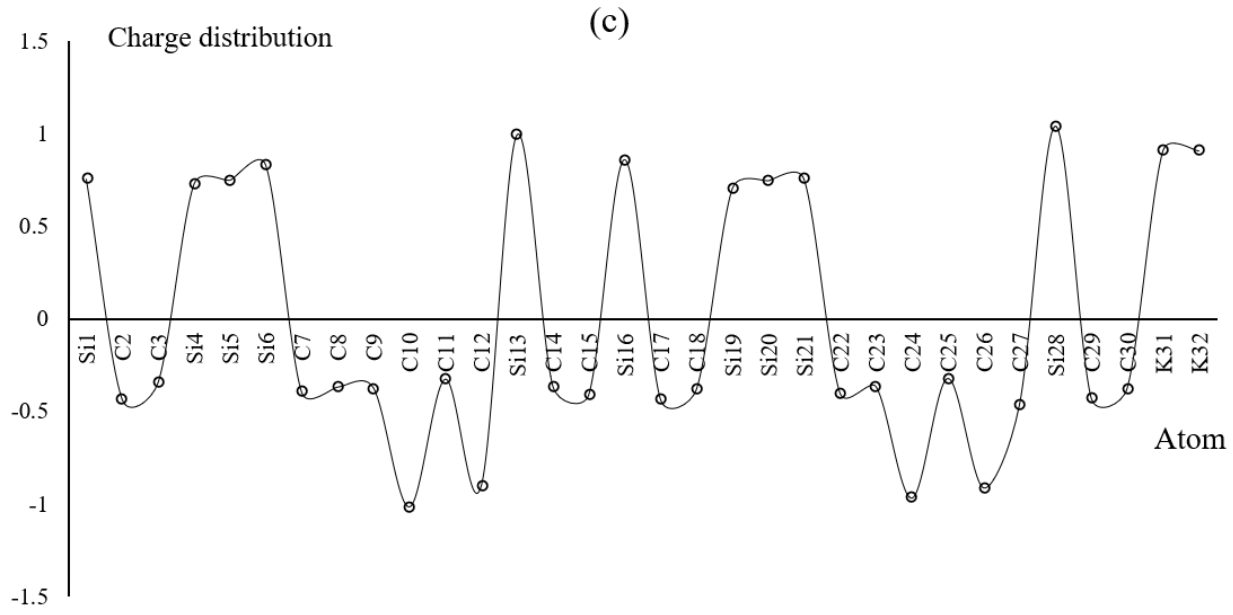


**Figure 3.**
The changes of charge distribution for (a) $Li_2(SiC)$, (b) $Na_2(SiC)$ and (c) $K_2(SiC)$ nanoclusters.

*3.2. Total Density of States*

In an isolated system (such as a molecule), the energy levels are discrete, and the concept of "density of states (DOS)" is completely valueless in this situation. Therefore, the "original total DOS (TDOS)" of an isolated system can be written as [23]:

$$TDOS\ (E) = \sum_i \delta\ (E - \epsilon_i\ ) \quad (1)$$

The normalized Gaussian function is defined as:

$$G(x) = \frac{1}{c\sqrt{2\pi}} e^{-\frac{x^2}{2c^2}} \quad \text{where} \quad c = \frac{\text{FWHM}}{2\sqrt{2\ln x}} \quad (2)$$

"FWHM (full width at half maximum)" is an adjustable parameter in "Multiwfn" [24, 25]. Furthermore, the curve maps of "broadened partial DOS (PDOS)" and "overlap DOS (OPDOS)" are valuable for visualizing orbital composition analysis; the "PDOS function of fragment *A"* is defined as:

$$PDOS_A\ (E) = \sum_i \Xi_{i,A}\ F\ (E - \epsilon_i\ ) \quad (3)$$

where" $\Xi_{i,A}$ is the composition of fragment *A* in orbital *i*. The "OPDOS between fragments *A* and *B*" is defined as:

$$OPDOS_{A,B}\ (E) = \sum_i X_{A,B}^i\ F\ (E - \epsilon_i\ ) \quad (4)$$

Where " $X_{A,B}^i$ is the composition of the total cross term between fragments *A* and *B* in orbital *i*.

In the "TDOS map," each discrete vertical line corresponds to a "molecular orbital (MO)," while the dashed line highlights the position of the "HOMO." The curve represents the "TDOS," simulated based on the distribution of "MO" energy levels.

Regarding energy storage by $Li_2(SiC)$, $Na_2(SiC)$, and $K_2(SiC)$ nanoclusters, the TDOS has been evaluated. This factor can demonstrate the existence of important chemical interactions, often on the "convex side"(Figure 4a,b,c).

*Edelweiss Applied Science and Technology*
*ISSN: 2576-8484*
*Vol. 10, No. 9: 157-173, 2026*
*DOI: 10.55214/2576-8484.v10i9.13563*

$Li_2(SiC)$, $Na_2(SiC)$, and $K_2(SiC)$ nanoclusters (Figure 4a,b,c) have shown the steepest TDOS maxima surrounding –0.30, –0.40, –0.50, and –0.60 a.u., owing to covalent bonds between the Li, Na, and K atoms and the SiC nanostructure, with a maximum density of states of approximately 12.

Fragment 1 was defined for C9 to C12, Si13, C24 to C27, Si28, and X31/X32 (X = Li, Na, K) in Figure 4 (a, b, c). Fragment 2 indicated the fluctuations of Si1 and Si4 to Si6, alongside the corresponding atoms of Fragment 1, in Figure 4 (a, b, c). Finally, the fluctuations of Si16, Si19 to Si21, C17, C18, C22, C23, C29, and C30 were considered in Figure 4 (a,b,c).

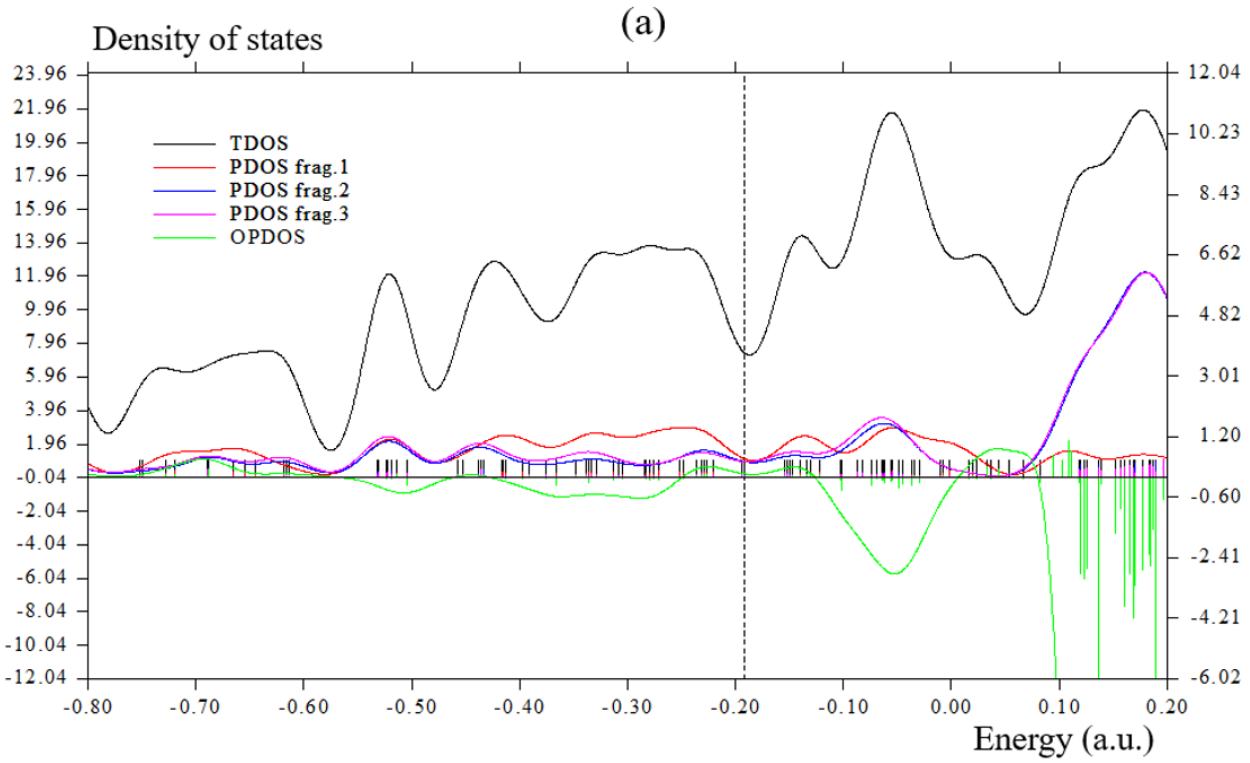


*Edelweiss Applied Science and Technology*
*ISSN: 2576-8484*
*Vol. 10, No. 9: 157-173, 2026*
*DOI: 10.55214/2576-8484.v10i9.13563*

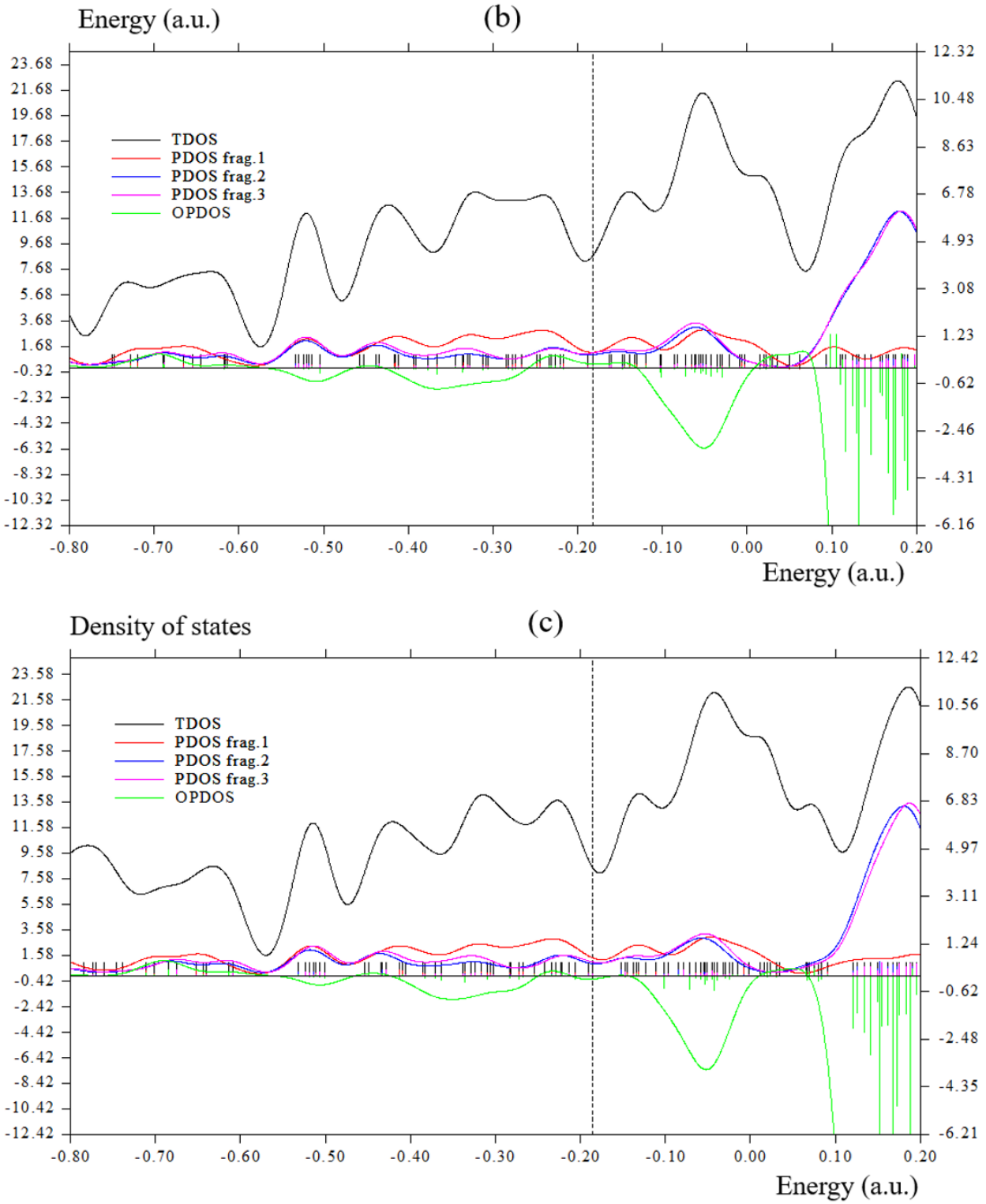


**Figure 4.**
OPDOS/PDOS/TDOS graphs of (a) $Li_2(SiC)$, (b) $Na_2(SiC)$ and (c) $K_2(SiC)$ nanoclusters.

*Edelweiss Applied Science and Technology*
*ISSN: 2576-8484*
*Vol. 10, No. 9: 157-173, 2026*
*DOI: 10.55214/2576-8484.v10i9.13563*

*3.3. Molecular Electrostatic Potential (ESP)*

Molecular electrostatic potential (ESP) has long been widely used for predicting nucleophilic and electrophilic sites. It is also valuable for studying hydrogen bonds, halogen bonds, molecular recognition, and intermolecular interactions involving aromatics [26]. This function measures the electrostatic interaction between a unit point charge placed at **r** and the system of interest. A positive (negative) value implies that the current position is dominated by nuclear (electronic) charges.

$$V_{tot}(r) = V_{nuc}(r) + V_{ele}(r) = \sum_A \frac{Z_A}{|r - R_A|} - \int \frac{\rho(r')}{|r - r'|} dr' \qquad (5)$$

$Z_A$ is the nuclear charge; if a pseudopotential is used, then $Z_A$ is the number of explicitly represented electrons. Notice that evaluating ESP is much more time-consuming than evaluating other functions. Also note that ESP in Multiwfn is evaluated exactly using nuclear-attraction integrals rather than approximate methods (such as multipole expansion or the numerical Poisson equation); hence, you may find that the results generated by Multiwfn differ somewhat from those output by other quantum chemistry codes. To speed up ESP evaluation, Multiwfn ignores some integrals that make little contribution. The threshold for ignoring them is controlled by "esppreciutoff" in settings.ini. Increasing this parameter results in more accurate ESP values but also incurs greater computational cost. ESP evaluated under the default value is generally accurate enough.

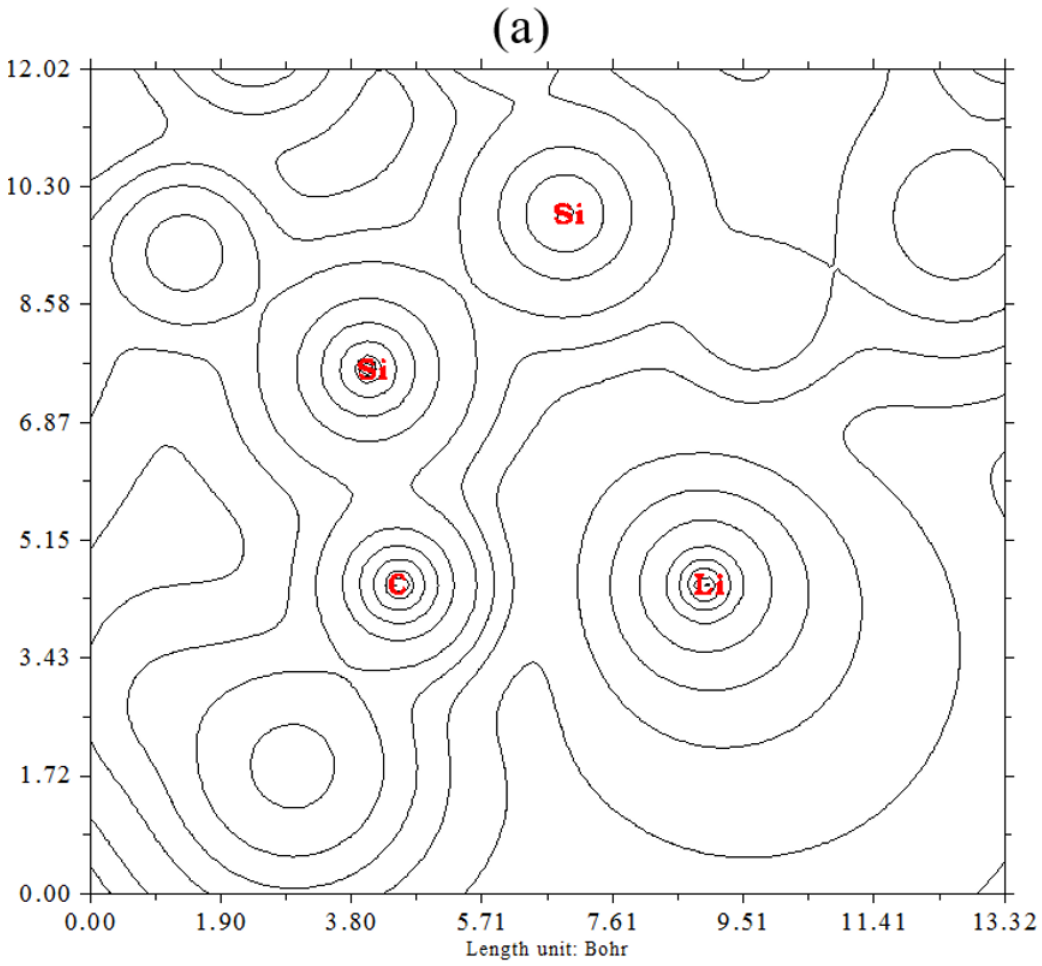


*Edelweiss Applied Science and Technology*
*ISSN: 2576-8484*
*Vol. 10, No. 9: 157-173, 2026*
*DOI: 10.55214/2576-8484.v10i9.13563*

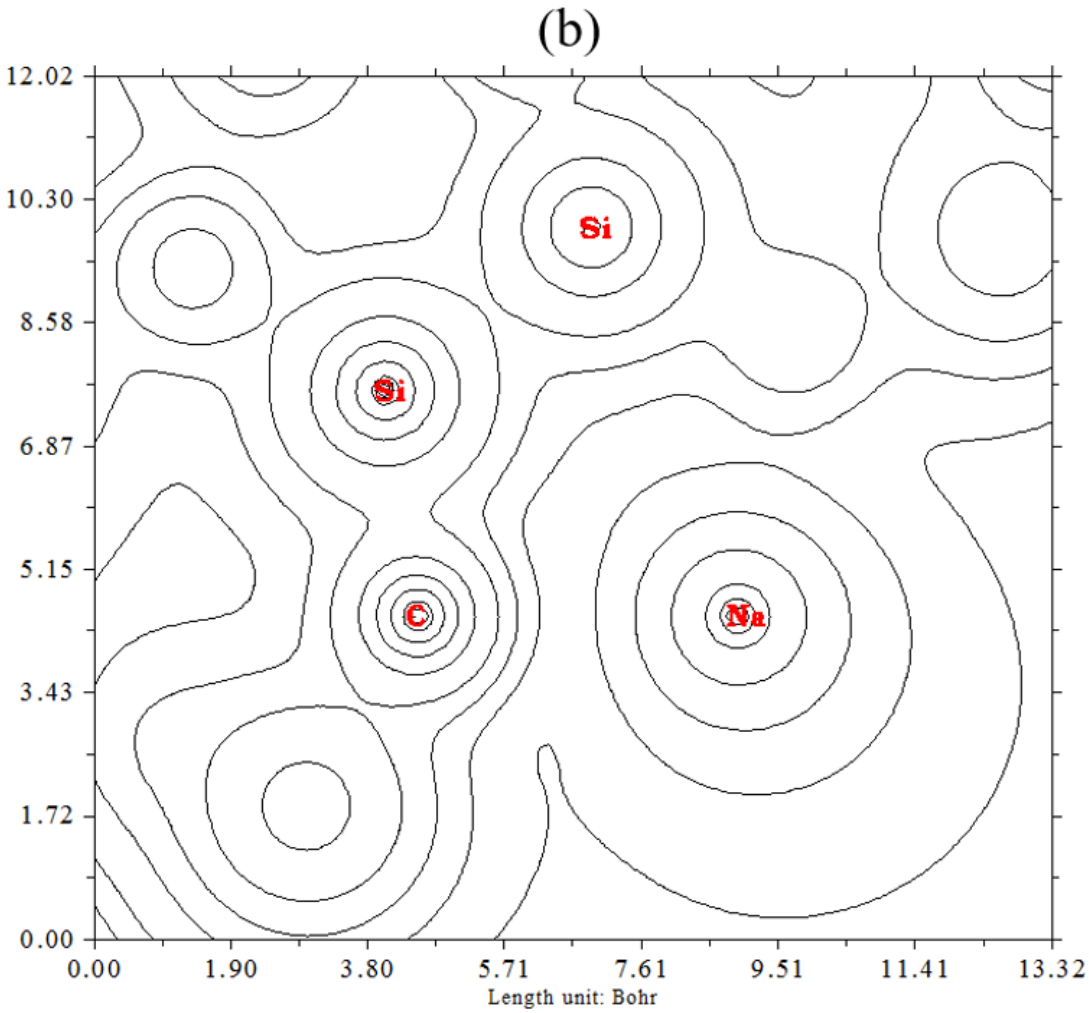


*Edelweiss Applied Science and Technology*
*ISSN: 2576-8484*
*Vol. 10, No. 9: 157-173, 2026*
*DOI: 10.55214/2576-8484.v10i9.13563*

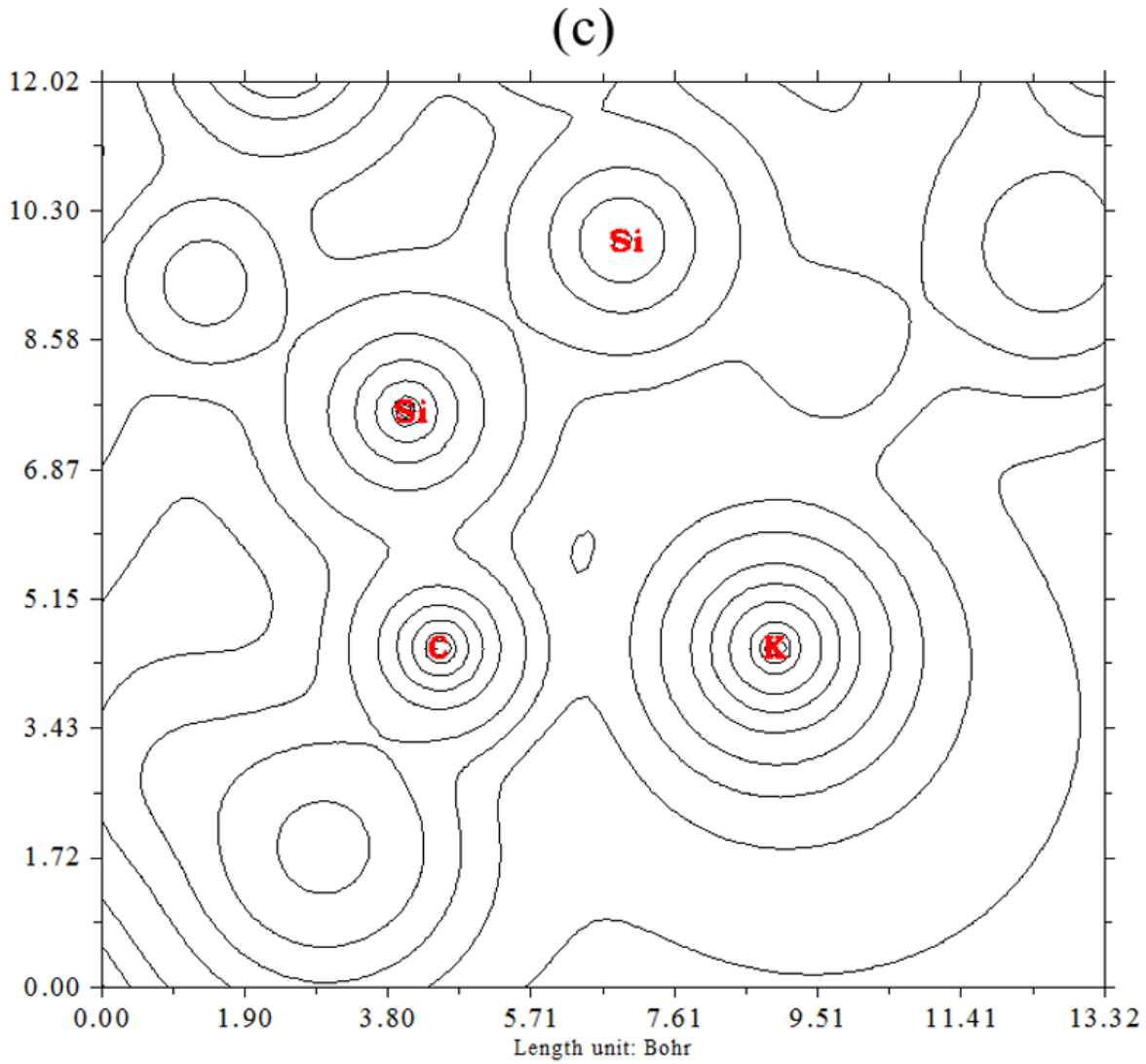


**Figure 5.**
The counter maps of ESP graphs for (a) $Li_2(SiC)$, (b) $Na_2(SiC)$, and (c) $K_2(SiC)$ nanoclusters.

The trapping of Li, Na, and K atoms by SiC nanostructures (Figure 5a,b,c), leading to the formation of $Li_2(SiC)$, $Na_2(SiC)$, and $K_2(SiC)$ nanoclusters, might be described using ESP graphs generated with Multiwfn [24, 25] because they reveal the delocalization/localization characteristics [27] of electrons and chemical bonds (Figure 5a,b,c).

$Li_2(SiC)$ (Figure 5a), $Na_2(SiC)$ (Figure 5b), and $K_2(SiC)$ (Figure 5c) have demonstrated electron delocalization through an isosurface map labeling the atoms C10, C12, Si13, C24, C26, Si28, and X31/X32 (X = Li, Na, K). In fact, the corresponding ESP map confirms that $Li_2(SiC)$, $Na_2(SiC)$, and $K_2(SiC)$ nanoclusters may enhance the efficiency of energy storage (Figure 5a,b,c).

Besides, the intermolecular orbital overlap integral is important for illustrating intermolecular charge transfer, which can be used to compute the HOMO–HOMO and LUMO–LUMO overlap integrals between Li, Na, and K atoms and the SiC nanostructure. The layered silicon carbide structures improved with the alkali metals lithium, sodium, and potassium have indicated the structural stability of Li-, Na-, and K-ion batteries through the reported stability energies in Table 2. Moreover, the

*Edelweiss Applied Science and Technology*
*ISSN: 2576-8484*
*Vol. 10, No. 9: 157-173, 2026*
*DOI: 10.55214/2576-8484.v10i9.13563*

intermolecular orbital overlap integral is important in discussions of intermolecular charge transfer, as it can be used to calculate the HOMO–HOMO and LUMO–LUMO overlap integrals between the alkali metals and silicon carbide. The wavefunction level we used was CAM–B3LYP–D3/6–311+G(d,p), which corresponds to the HOMO and LUMO, respectively (Table 2). Therefore, $E_{LUMO}$ (a.u.), $E_{LUMO}$ (a.u.), the local bandgap energies (ΔE/a.u.), and the immobile charges induced by polarization discontinuity are simultaneously controlled throughout the structures, and optimized band profiles are eventually achieved for $Li_2$(SiC), $Na_2$(SiC), and $K_2$(SiC) nanoclusters (Table 2). A small portion of Li, Na, or K entering the Si–C layer to replace the alkali-metal sites could improve the structural stability of the electrode material at high multiplicity, thereby improving the capacity retention rates to 100.2018, 94.5295, 198.8630, and 188.1862 $mAhg^{-1}$ for the $Li_2$(SiC), $Na_2$(SiC), and $K_2$(SiC) complexes, respectively (Table 2).

**Table 2.**
Stability energy (kcal/mol), dipole moment (debye), LUMO (eV), HOMO(eV), energy gap (ΔE) (eV), and cell capacity (C, mAh $g^{-1}$ ) for $Li_2$(SiC), $Na_2$(SiC), and $K_2$(SiC) nanoclusters.

| Heteroclusters | $E_a \times 10^{-3}$ (kcal/mol) | Dipole moment (Debye) | $E_{HOMO}$ (eV) | $E_{LUMO}$ (eV) | $\Delta E = E_{LUMO} - E_{HOMO}$ (eV) | C (C, mAh $g^{-1}$ ) |
|---|---|---|---|---|---|---|
| $Li_2$(SiC) | -509.2147 | 1.2501 | -5.2061 | -4.2002 | 1.006 | 100.2018 |
| $Na_2$(SiC) | -499.9578 | 1.1864 | -4.9625 | -4.4375 | 0.525 | 94.5295 |
| $K_2$(SiC) | -534.8313 | 0.9438 | -5.0568 | -4.1293 | 0.9275 | 453.141 |

In addition, the Mayer bond order [28] is generally consistent with the empirical bond order for a single bond, which is near 1.0. The Mulliken bond order [29], which shows little agreement with the empirical bond order, is not appropriate for quantifying bonding strength; Mayer bond order generally performs better. However, the Mulliken bond order is a good qualitative indicator of the positive contribution of bonding and the negative contribution of antibonding, which are delocalized and localized, respectively (Table 3). As seen in Table 3, the Laplacian bond order [30] has a direct correlation with bond polarity, bond dissociation energy, and bond vibrational frequency. The low value of the Laplacian bond order might indicate that it is insensitive to the level of calculation used to generate the electron density. Generally, the value of the Fuzzy bond order is close to that of the Mayer bond order, especially for low-polarity bonds, but is much more stable with respect to changes in the basis set. Computing the Fuzzy bond order requires Becke's DFT numerical integration; therefore, its computational cost is higher than that of the Mayer bond order, and it can represent bonding more precisely [31].

*Edelweiss Applied Science and Technology*
*ISSN: 2576-8484*
*Vol. 10, No. 9: 157-173, 2026*
*DOI: 10.55214/2576-8484.v10i9.13563*

**Table 3.**
The bond order of Mayer, Wiberg, Mulliken, Laplacian, and Fuzzy from mixed alpha and beta density matrices for $Li_2(SiC)$, $Na_2(SiC)$, and $K_2(SiC)$ nanoclusters.

| Compound | Bond type | Bond order | | | | |
|---|---|---|---|---|---|---|
| | | Mayer | Wiberg | Mulliken | Laplacian | Fuzzy |
| $Li_2(SiC)$ | Si13–Si28 | 0.7326 | 0.6774 | 0.5663 | 2.1165 | 0.9021 |
| | C10–Li32 | 0.4060 | 0.4238 | 0.4781 | 0.4291 | 0.3601 |
| | C12–Li31 | 0.1585 | 0.2653 | 0.2721 | 0.276 | 0.1806 |
| | C24–Li32 | 0.3640 | 0.4079 | 0.4470 | 0.4210 | 0.3380 |
| | C26–Li31 | 0.2071 | 0.3148 | 0.3086 | 0.3981 | 0.2241 |
| $Na_2(SiC)$ | Si13–Si28 | 0.6976 | 0.6677 | 0.4213 | 0.4721 | 0.8714 |
| | C10–Na32 | 0.4105 | 0.2761 | 0.5937 | 0.5892 | 0.5296 |
| | C12–Na31 | 0.1593 | 0.2012 | 0.3233 | 0.3094 | 0.3348 |
| | C24–Na32 | 0.4085 | 0.2766 | 0.5589 | 0.5341 | 0.5171 |
| | C26–Na31 | 0.2187 | 0.2314 | 0.3734 | 0.3617 | 0.3887 |
| $K_2(SiC)$ | Si13–Si28 | 0.7615 | 0.6675 | 0.9743 | 0.9326 | 0.8594 |
| | C10–K32 | 0.5690 | 0.3913 | 0.5413 | 0.5301 | 0.5890 |
| | C12–K31 | 0.2461 | 0.2376 | 0.1143 | 0.1038 | 0.3540 |
| | C24–K32 | 0.5804 | 0.3860 | 0.4209 | 0.4061 | 0.5830 |
| | C26–K31 | 0.3619 | 0.2928 | 0.2040 | 0.1953 | 0.4223 |

## 4. Conclusions

The capture of alkali metals by silicon carbide, leading to the formation of $Li_2(SiC)$, $Na_2(SiC)$, and $K_2(SiC)$ nanoclusters, was studied computationally. Changes in charge density indicated notable charge transfer in $Li_2(SiC)$, $Na_2(SiC)$, and $K_2(SiC)$. Due to the semiconducting nature of SiC, it is usually composited with C to achieve better ionic and electronic conductivity. It is well established that adding Li, Na, or K to cell batteries can augment their energy storage. The results of this research article demonstrate that the architectural design of $X_2(SiC)$ (X = Li, Na, K) can augment the capacity of battery cells. A small portion of Li, Na, or K entering the Si–C layer to replace alkali-metal sites could improve the structural stability of the electrode material at high multiplicity, thereby improving the capacity retention rates to 100.2018, 94.5295, 198.8630, and 188.1862 $mAhg^{-1}$ for the $Li_2(SiC)$, $Na_2(SiC)$, and $K_2(SiC)$ complexes, respectively. This research article is useful for designing and constructing Li, Na, or K hybrid batteries with high power and energy densities and excellent cycle stability, and it provides a perspective on the industrial application of these hybrid batteries.

## Transparency:

The authors confirm that the manuscript is an honest, accurate, and transparent account of the study; that no vital features of the study have been omitted; and that any discrepancies from the study as planned have been explained. This study followed all ethical practices during writing.


## Acknowledgements:

The authors are grateful to Kastamonu University for completing this paper and its research.




## References


[1] X. Fan, D. Deng, Y. Li, and Q.-H. Wu, "Recent progress in SiC nanostructures as anode materials for lithium-ion batteries," *Current Materials Science: Formerly: Recent Patents on Materials Science*, vol. 16, no. 1, pp. 18-29, 2023. https://doi.org/10.2174/2666145415666220822120615

[2] X. Zhao and V.-P. Lehto, "Challenges and prospects of nanosized silicon anodes in lithium-ion batteries," *Nanotechnology*, vol. 32, no. 4, p. 042002, 2021. https://doi.org/10.1088/1361-6528/abb850

[3] Q. Wen, F. Qu, Z. Yu, M. Graczyk-Zajac, X. Xiong, and R. Riedel, "Erratum to: Si-based polymer-derived ceramics for energy conversion and storage," *Journal of Advanced Ceramics*, vol. 11, no. 6, pp. 984-984, 2022. https://doi.org/10.1007/s40145-022-0600-8

[4] M. Ge *et al.*, "Recent advances in silicon-based electrodes: From fundamental research toward practical applications," *Advanced Materials*, vol. 33, no. 16, p. 2004577, 2021. https://doi.org/10.1002/adma.202004577

[5] G. Shao *et al.*, "Polymer-derived SiOC integrated with a graphene aerogel as a highly stable Li-ion battery anode," *ACS Applied Materials & Interfaces*, vol. 12, no. 41, pp. 46045-46056, 2020. https://doi.org/10.1021/acsami.0c12376

[6] G. Mera, A. Navrotsky, S. Sen, H.-J. Kleebe, and R. Riedel, "Polymer-derived SiCN and SiOC ceramics–structure and energetics at the nanoscale," *Journal of Materials Chemistry A*, vol. 1, no. 12, pp. 3826-3836, 2013. https://doi.org/10.1039/c2ta00727d

[7] M. Wilamowska-Zawlocka *et al.*, "Silicon oxycarbide ceramics as anodes for lithium ion batteries: Influence of carbon content on lithium storage capacity," *RSC Advances*, vol. 6, no. 106, pp. 104597-104607, 2016. https://doi.org/10.1039/c6ra24539k

[8] V. Pradeep, D. G. Ayana, M. Graczyk-Zajac, G. D. Soraru, and R. Riedel, "High rate capability of SiOC ceramic aerogels with tailored porosity as anode materials for Li-ion batteries," *Electrochimica Acta*, vol. 157, pp. 41-45, 2015. https://doi.org/10.1016/j.electacta.2015.01.088

[9] Q. Liu *et al.*, "Graphitic SiC: A potential anode material for Na-ion battery with extremely high storage capacity," *International Journal of Quantum Chemistry*, vol. 121, no. 10, p. e26608, 2021. https://doi.org/10.1002/qua.26608

[10] Q. Peng *et al.*, "Anchoring of K and Na on the surface of a novel SiC monolayer: First-principles predictions," *Journal of Energy Storage*, vol. 104, p. 114435, 2024. https://doi.org/10.1016/j.est.2024.114435

[11] A. A. Khan, R. Ahmad, and I. Ahmad, "Silicon carbide and III-Nitrides nanosheets: Promising anodes for Mg-ion batteries," *Materials Chemistry and Physics*, vol. 257, p. 123785, 2021. https://doi.org/10.1016/j.matchemphys.2020.123785

[12] N. Yodsin, H. Sakagami, T. Udagawa, T. Ishimoto, S. Jungsuttiwong, and M. Tachikawa, "Metal-doped carbon nanocones as highly efficient catalysts for hydrogen storage: Nuclear quantum effect on hydrogen spillover mechanism," *Molecular Catalysis*, vol. 504, p. 111486, 2021. https://doi.org/10.1016/j.mcat.2021.111486

[13] H. O. Taha, A. M. El Mahdy, F. E. S. El Shemy, and M. M. Hassan, "Hydrogen storage in SiC, GeC, and SnC nanocones functionalized with nickel, density functional theory—study," *International Journal of Quantum Chemistry*, vol. 123, no. 3, p. e27023, 2023. https://doi.org/10.1002/qua.27023

[14] T. Wei *et al.*, "An intermittent lithium deposition model based on CuMn-bimetallic MOF derivatives for composite lithium anode with ultrahigh areal capacity and current densities," *Nano Research*, vol. 17, pp. 2763-2769, 2024. https://doi.org/10.1007/s12274-023-6187-8

[15] F. Mollaamin and M. Monajjemi, "Nanomaterials for sustainable energy in hydrogen-fuel cell: Functionalization and characterization of carbon nano-semiconductors with silicon, germanium, tin or lead through density functional theory study," *Russian Journal of Physical Chemistry B*, vol. 18, no. 2, pp. 607-623, 2024. https://doi.org/10.1134/S1990793124020271

[16] F. Mollaamin, S. Shahriari, and M. Monajjemi, "Influence of transition metals for emergence of energy storage in fuel cells through hydrogen adsorption on the MgAl surface," *Russian Journal of Physical Chemistry B*, vol. 18, pp. 398-418, 2024. https://doi.org/10.1134/S199079312402026X

[17] F. Mollaamin, "Competitive intracellular hydrogen-nanocarrier among aluminum, carbon, or silicon implantation: A novel technology of eco-friendly energy storage using research density functional theory," *Russian Journal of Physical Chemistry B*, vol. 18, pp. 805-820, 2024. https://doi.org/10.1134/S1990793124700131

[18] H. Che *et al.*, "Rubidium and cesium ions as electrolyte additive for improving performance of hard carbon anode in sodium-ion battery," *Electrochemistry Communications*, vol. 83, pp. 20-23, 2017. https://doi.org/10.1016/j.elecom.2017.08.012

[19] G. Henkelman, A. Arnaldsson, and H. Jónsson, "A fast and robust algorithm for Bader decomposition of charge density," *Computational Materials Science*, vol. 36, no. 3, pp. 354-360, 2006. https://doi.org/10.1016/j.commatsci.2005.04.010

[20] M. J. Frisch, G. W. Trucks, H. B. Schlegel, G. E. Scuseria, and M. A. Robb, *Gaussian 16, Revision C.01*. Wallingford CT: Gaussian, Inc, 2016.

[21] R. Dennington, T. A. Keith, and J. M. Millam, *GaussView, version 6.0.16*. Shawnee Mission, KS, USA: Semichem Inc, 2016.

[22] Z. Xu, C. Qin, Y. Yu, G. Jiang, and L. Zhao, "First-principles study of adsorption, dissociation, and diffusion of hydrogen on α-U (110) surface," *AIP Advances*, vol. 14, no. 5, p. 055114, 2024. https://doi.org/10.1063/5.0208082

[23] F. Mollaamin and M. Monajjemi, "Designing novel nanomaterials for Li-ion batteries: A physico-chemical study through hydrogen-powered horizons," *New Materials, Compounds and Applications*, vol. 8, no. 3, pp. 303-323, 2024. https://doi.org/10.62476/nmca83303

[24] T. Lu and F. Chen, "Multiwfn: A multifunctional wavefunction analyzer," *Journal of Computational Chemistry*, vol. 33, no. 5, pp. 580-592, 2012. https://doi.org/10.1002/jcc.22885

[25] T. Lu, "A comprehensive electron wavefunction analysis toolbox for chemists, Multiwfn," *The Journal of Chemical Physics*, vol. 161, no. 8, p. 082503, 2024. https://doi.org/10.1063/5.0216272

[26] J. S. Murray and P. Politzer, "The electrostatic potential: An overview," *Wiley Interdisciplinary Reviews: Computational Molecular Science*, vol. 1, no. 2, pp. 153-163, 2011. https://doi.org/10.1002/wcms.19

[27] C. F. Matta, P. W. Ayers, and R. Cook, *The physics of electron localization and delocalization. In Electron Localization-Delocalization Matrices*. Cham: Springer International Publishing, 2024.

[28] I. Mayer, "Improved definition of bond orders for correlated wave functions," *Chemical Physics Letters*, vol. 544, pp. 83-86, 2012. https://doi.org/10.1016/j.cplett.2012.07.003

[29] F. Mollaamin, M. Baei, M. Monajjemi, R. Zhiani, and B. Honarparvar, "A DFT study of hydrogen chemisorption on V (100) surfaces," *Russian Journal of Physical Chemistry A, Focus on Chemistry*, vol. 82, pp. 2354-2361, 2008. https://doi.org/10.1134/S0036024408130323

[30] T. Lu and F. Chen, "Bond order analysis based on the Laplacian of electron density in fuzzy overlap space," *The Journal of Physical Chemistry A*, vol. 117, no. 14, pp. 3100-3108, 2013. https://doi.org/10.1021/jp4010345

[31] X. Wang, X. Zhang, W. Pedrycz, S.-H. Yang, and D. Boutat, "Consensus of TS fuzzy fractional-order, singular perturbation, multi-agent systems," *Fractal and Fractional*, vol. 8, no. 9, p. 523, 2024. https://doi.org/10.3390/fractalfract8090523

*Edelweiss Applied Science and Technology*
*ISSN: 2576-8484*
*Vol. 10, No. 9: 157-173, 2026*
*DOI: 10.55214/2576-8484.v10i9.13563*